Abrupt climate variability since the last deglaciation based on a high-resolution, multi-proxy peat record from NW Iran: The hand that rocked the Cradle of Civilization?

Arash Sharifi [a, b, *], Ali Pourmand [a, b], Elizabeth A. Canuel [c], Erin Ferer-Tyler [c], Larry C. Peterson [b], Bernhard Aichner [d], Sarah J. Feakins [d], Touraj Daryaee [e], Morteza Djamali [f], Abdolmajid Naderi Beni [g], Hamid A.K. Lahijani [g], Peter K. Swart [b]

[a] Neptune Isotope Laboratory (NIL), Department of Marine Geosciences, Rosenstiel School of Marine and Atmospheric Science, University of Miami, 4600 Rickenbacker Causeway, Miami, FL 33149-1098, USA
[b] Department of Marine Geosciences, Rosenstiel School of Marine and Atmospheric Science (RSMAS), University of Miami, 4600 Rickenbacker Causeway, Miami, FL 33149-1098, USA
[c] Virginia Institute of Marine Science, College of William & Mary, P.O. Box 1346, Gloucester Point, VA, USA
[d] University of Southern California, Department of Earth Sciences, 3651 Trousdale Pkwy, Los Angeles, CA 90089-0740, USA
[e] Samuel M. Jordan Center for Persian Studies and Culture at the University of California, Irvine, CA 92697, USA
[f] Institut Méditerranéen de biodiversité et d'Ecologie (IMBE — UMR CNRS 7263 / IRD 237), Europôle Méditerranéen de l'Arbois, BP 80, 13545 Aix-en-Provence cedex 04, France
[g] Iranian National Institute for Oceanography and Atmospheric Science (INIOAS), Marine Geology Division, P.O. Box 14155-4781 Tehran, Iran

ARTICLE INFO

ABSTRACT

We present a high-resolution (sub-decadal to centennial), multi-proxy reconstruction of aeolian input and changes in palaeohydrological conditions based on a 13000 Yr record from Neor Lake's peripheral peat in NW Iran. Variations in relative abundances of refractory (Al, Zr, Ti, and Si), redox sensitive (Fe) and mobile (K and Rb) elements, total organic carbon (TOC), $\delta^{13}C_{TOC}$, compound-specific leaf wax hydrogen isotopes (δD), carbon accumulation rates and dust fluxes presented here fill a large gap in the existing terrestrial paleoclimate records from the interior of West Asia. Our results suggest that a transition occurred from dry and dusty conditions during the Younger Dryas (YD) to a relatively wetter period with higher carbon accumulation rates and low aeolian input during the early Holocene (9000—6000 Yr BP). This period was followed by relatively drier and dustier conditions during middle to late Holocene, which is consistent with orbital changes in insolation that affected much of the northern hemisphere. Numerous episodes of high aeolian input spanning a few decades to millennia are prevalent during the middle to late Holocene. Wavelet analysis of variations in Ti abundances as a proxy for aeolian input revealed notable periodicities at 230, 320, and 470 years with significant periodicities centered around 820, 1550, and 3110 years over the last 13000 years. Comparison with palaeoclimate archives from West Asia, the North Atlantic and African lakes point to a teleconnection between North Atlantic climate and the interior of West Asia during the last glacial termination and the Holocene epoch.

We further assess the potential role of abrupt climate change on early human societies by comparing our record of palaeoclimate variability with historical, geological and archaeological archives from this region. The terrestrial record from this study confirms previous evidence from marine sediments of the Arabian Sea that suggested climate change influenced the termination of the Akkadian empire. In addition, nearly all observed episodes of enhanced dust deposition during the middle to late Holocene coincided with times of drought, famine, and power transitions across the Iranian Plateau, Mesopotamia and the eastern Mediterranean region. These findings indicate that while socio-economic factors are traditionally considered to shape ancient human societies in this region, the influence of abrupt climate change should not be underestimated.

* Corresponding author. Neptune Isotope Laboratory (NIL), Department of Marine Geosciences, Rosenstiel School of Marine and Atmospheric Science, University of Miami, 4600 Rickenbacker Causeway, Miami, FL 33149-1098, USA.
E-mail address: osharifi@rsmas.miami.edu (A. Sharifi).

1. Introduction

Since the beginning of the Neolithic Era, the area in West Asia that extends from southwestern Iran and the Arabian Peninsula to the eastern and southeastern Mediterranean Sea, also referred to as the "Cradle of Civilization" and the "Fertile Crescent", has witnessed the birth of agriculture and development of some of the earliest human societies (Leick, 2010; Mellaart, 1975; Riehl et al., 2013). Evidence is mounting that abrupt climate change during the Holocene epoch (beginning 11700 before present, BP) may have played a transformative role in the growth and deterioration of human civilizations (Brooks, 2006; Cullen et al., 2000; deMenocal, 2001; Riehl, 2009). Although the amplitude of climate variability was reduced during the Holocene relative to the last glacial period (Grootes et al., 1993), episodes of abrupt climatic change have been documented in marine and terrestrial records throughout the Holocene in both hemispheres (see review by Mayewski et al., 2004).

On a regional scale, the climate of West Asia is governed by complex interactions between the mid-latitude Westerlies, the Siberian Anticyclone and the Indian Ocean Summer Monsoon (Fig. 1). While a number of paleoclimate studies have drawn potential links between abrupt climate change and the rise and fall of civilizations across the Fertile Crescent (Cullen et al., 2000; Staubwasser and Weiss, 2006), high-resolution (sub-decadal to centennial) terrestrial archives of climate variability with well-constrained age models are scarce from this region (Nicoll and Küçükuysal, 2013). Such records are needed in order to address the uncertainty regarding the timing and regional significance of climatic transitions and their potential influence on early human societies, and the extent to which anthropogenic activities may have influenced the climate of the last deglacial period.

Interpreting the available proxy reconstructions of Holocene climate variability in the interior of West Asia is not straightforward. For example, Stevens et al. (2001) found disagreement between relatively lower $\delta^{18}O$ values from Lake Zeribar during the early Holocene, which are generally interpreted to represent wetter conditions (Roberts et al., 2008), and pollen and macrofossil data for this period from Lake Zeribar, which were interpreted to indicate drier conditions during this period. They concluded that lower $\delta^{18}O$ values may have been due to a shift in the timing of precipitation (i.e., protracted summers). Other explanations that have been suggested for this discrepancy include underestimating human impact on vegetation during the early Holocene, and the delayed reaction of biomes to postglacial climate change (Djamali et al., 2010; Roberts, 2002). Stevens et al. (2006) further examined geochemical and biological evidences from Lake Mirabad in western Iran during this period and concluded that the early Holocene was dry. Based on microfossil assemblages and pollen data, Wasylikowa et al. (2006) concluded that Zeribar lake levels were variable during the early Holocene. Pollen and ostracod assemblages from lakes in Turkey, Iran and Georgia suggest that continental (dry and variable) climate dominated over the interior of West Asia during the early to middle Holocene (Connor and Kvavadze, 2008; El-Moslimany, 1982; Griffiths et al., 2001; Wasylikowa, 2005). Available records of palaeo-vegetation changes, however, fall short of disentangling human *versus* climate impact (Djamali et al., 2009a), indicating the need for high-resolution palaeoclimate reconstructions that are independent of vegetation types that may have been influenced by agriculture as well as climate (Roberts et al., 2011).

In this contribution, we present inorganic and organic proxy reconstruction of aeolian input and palaeohydrological changes over the last 13000 Yr from an ombrotrophic (rain fed) peat mire located at the periphery of Neor Lake in NW Iran. We examine the possibility of an atmospheric teleconnection during the last glacial termination and the Holocene by comparing our results with records from the North Atlantic, African lakes and eastern Mediterranean. We further investigate the potential influence of abrupt climate change on major early human societies from West Asia by comparing our findings with historical and archaeological records from this region.

2. Study area

Neor Lake (37°57′37″ N, 48°33′19″ E) is a seasonally recharged body of water formed over a tectonic depression on the leeward flank of the Talesh (Alborz) Mountains in NW Iran (Fig. 1 and Fig 2A). The tectonic depression, which formed within an andesitic bedrock as a result of displacements during the Eocene (Madadi et al., 2005) does not receive water from any permanent rivers and has fostered a peripheral peat mire in primarily southern section of the lake for at least the last 13000 years. Precipitation in this high-altitude peat mire (~2500 m above sea level, m.a.s.l.) consists of rain and snow. Water leaves the lake through an incision in the north that has been artificially dammed for the last few decades. The lake surface area is reduced by more than 50% during periods of low precipitation (Fig. 2B) (Madadi et al., 2005). Mass accumulation in the peat mire is primarily driven by accretion of decomposing biomass and wet and dry aeolian deposition.

The mean annual precipitation (30-years average) recorded at the nearest meteorological station in Ardebil, located at 1332 m.a.s.l. and 50 km NE of the lake, exceeds 300 mm. Precipitation is highest in May and November (Fig. 2B) and the dry season lasts from July to September. Mean annual temperature at the station is 15.4 °C and the mean maximum and minimum temperatures of the warmest and coldest months of the year are 25 °C (July) and −7.9 °C (January), respectively. As Neor peat mire is 1200 m higher than the meteorological station, it is not unreasonable to expect higher annual precipitation and lower temperature at Neor relative to the weather station. Vegetation in the lake basin is composed of Irano-Turanian mountain steppe, dominated by thorny-cushions plants. Local nomado-pastoral communities exploit both the steppe and the Neor peat mire vegetation.

3. Materials and methods

3.1. Peat cores

In the summer of 2010, we recovered a 7.5-m core from the southwest part of Neor peat mire (Fig. 1), as well as two additional cores of similar length from within 2 m of the main core. Half-barrel cores were collected in 1-m increments of 7-cm diameter using a Russian split corer until the basal bedrock was reached. The final segment of the core included dense, laminated gyttja and a mixture of andesitic gravel from the bedrock. The cores were photographed on site and transferred into PVC core liners, sealed in non-reactive plastic sheets and stored at 4 °C and constant humidity at the core repository of the Rosenstiel School of Marine and Atmospheric Science (RSMAS), the University of Miami. The physical properties of the core segments were logged, and changes in core dimensions were closely monitored throughout the course of the study as peat water content tended to vary with time. Each core segment was transferred into an especially-designed polymethyl methacrylate core holder and PVC liner with scale bars for reference. The cores were subsequently imaged using a Geotek Multi-Sensor Core Logger (GeotekMSCL) at the Department of Marine Geosciences (MGS), RSMAS and the images were calibrated for cross-core resolution, light intensity and white balance. The position of each sample taken for discrete organic and inorganic geochemical analyses was determined based on comparing down-core XRF
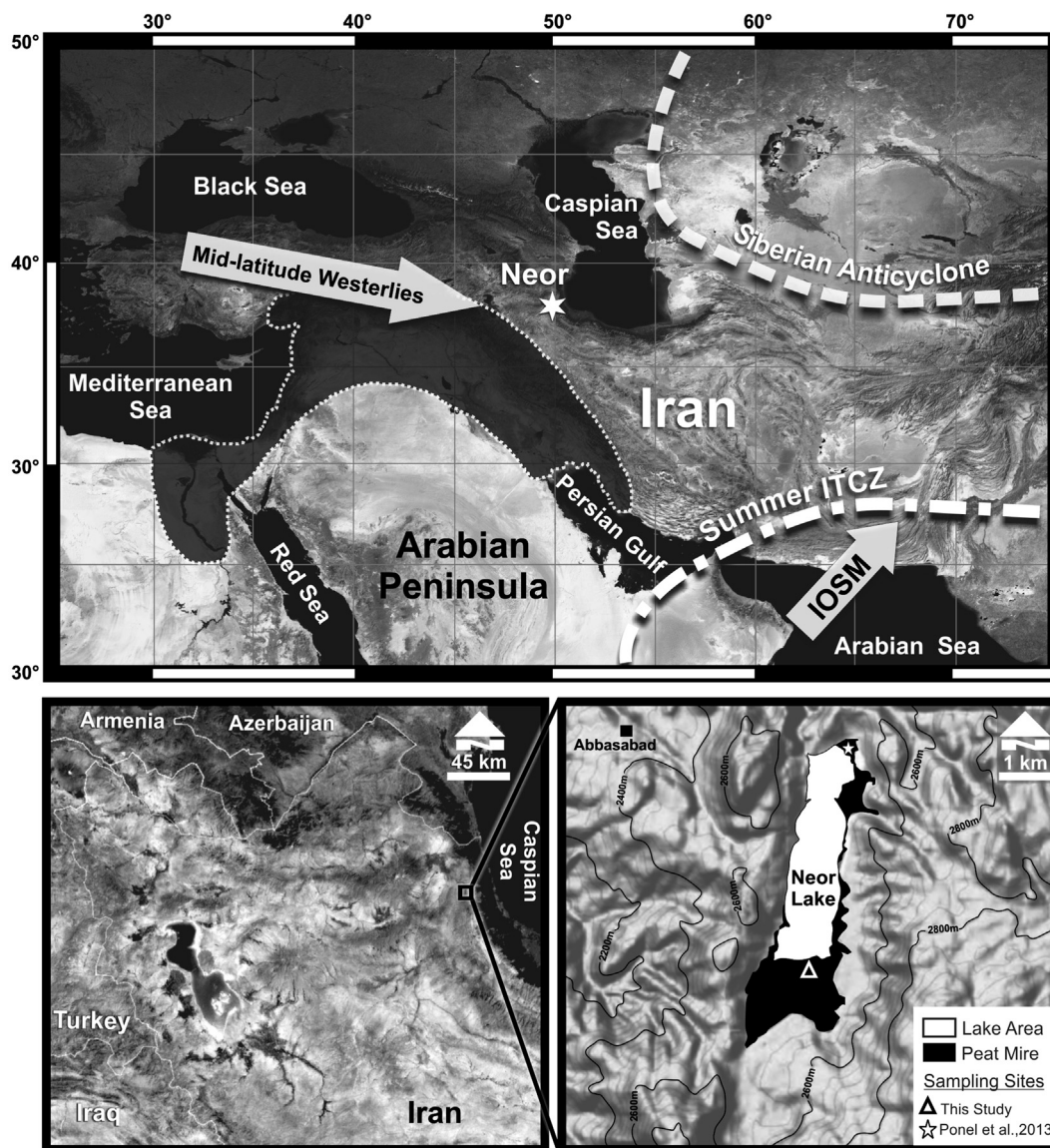
Fig. 1. Schematic position of major synoptic systems over West Asia and the location of Neor peat mire (star). Shaded area marks the region known as the "Fertile Crescent". The approximate current location of the Intertropical Convergence Zone (ITCZ) is also shown. IOSM refers to Indian Ocean Summer Monsoon. The Neor Lake's catchment basin and peripheral peat mire are shown in the bottom panel. Open triangle denotes the location of the peat core for this study.

elemental intensities and core images. Samples were taken from areas of high terrigenous input, which correspond to high XRF intensities, areas of high organic content with low XRF intensities as well as midpoints in order to capture the entire range of variability and minimize the effect of aliasing. Sub-samples were taken for organic and inorganic geochemical analyses using a pre-cleaned ceramic knife and the samples were dried at 45 °C over 5 days. The water content was measured for each sample gravimetrically based on sample masses before and after evaporation. The sampling resolution of each proxy record is discussed in sections 3.3–3.9.

3.2. Age model

Based on variations in the intensity of lithogenic elements measured by XRF (see section 3.3. below), 19 sub-samples were submitted for ^{14}C dating to the National Ocean Sciences Accelerator Mass Spectrometry Facility (NOSAMS), Woods Hole Oceanographic Institution. At NOSAMS, samples were pretreated using acid-only

or acid-base-acid protocols prior to graphitization based on their organic contents. Ages were based on ^{14}C analysis and associated uncertainties were calibrated using CALIB 6.0 program (Stuiver et al., 1998) by utilizing IntCal13 calibration dataset (Reimer et al., 2013). Ages are reported as calibrated year before present (cal. Yr BP).

3.3. Major and trace element analysis by XRF scanning

High-resolution measurements of the relative abundances of trace and major elements were performed on an AVAATECH XRF-core scanner in the Palaeoclimatology Lab at MGS-RSMAS. All core sections were scanned twice (10 kV, 1000 μA, no filter; 30 kV, 1000 μA, Pd filter) to acquire the range of elements reported here. For all measurements, the surface area was irradiated for 20 s of integration time at 2-mm intervals (average resolution of 3.5 yr) using a window 2-mm high by 12-mm wide. The raw XRF spectra were then processed using the Canberra WinAxil software with standard software settings and spectrum-fit models, and
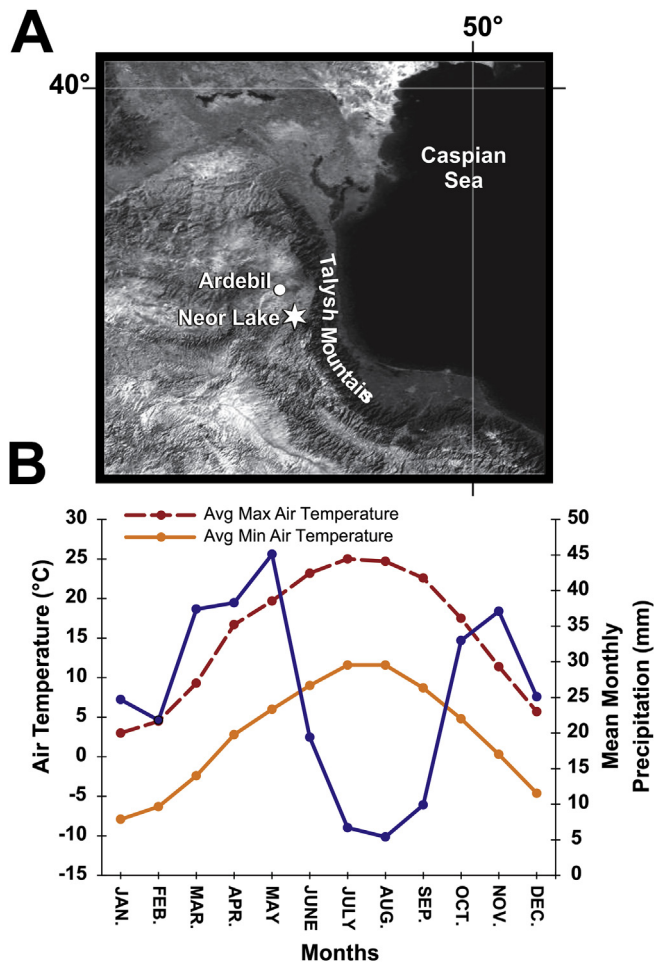
Fig. 2. A) Location of Neor peat mire with respect to Talysh (Alborz) Mountains. B) 30-year average of minimum and maximum monthly mean air temperature (dark red and yellow lines) and mean monthly precipitation (blue line) as recorded in Ardebil meteorological station.

abundances are reported as the intensity of each element in counts per second (cps). The JR-1 standard (Geological Survey of Japan) was used for calibration, and calibrated data were compared with previous measurements to check for discrepancies. We interpret the XRF elemental abundances as a qualitative proxy for changes in atmospheric dust input throughout the core. In addition, we calculated aeolian fluxes based on discrete analysis of Ti concentrations from a sub-set of 60 samples that corresponded to intervals of high, intermediate and low Ti intensities from XRF measurements and the bulk dry density of the peat core as described below.

3.4. Bulk density

Bulk density of peat material is required for quantifying atmospheric deposition. However, accurate measurement of bulk density in peat and poorly consolidated sediment is challenging. As a result, bulk density of sediments is often assumed to be constant in the sedimentary record or is measured on discrete samples using destructive gravimetric and volumetric techniques (Boelter, 1966; Chambers et al., 2011; Janssens, 1983). In addition to sample loss, this approach is not suitable for organic-rich sediments with high porosity.

We utilized a novel, alternative approach using Gamma Ray Attenuation Porosity Evaluator (GRAPE) data (Evans, 1965). The

bulk density based on gamma ray attenuation measurements as part of the GEOTEK-MSCL is calculated from the following equation:

$$\rho = \frac{1}{\mu d} ln \frac{I_0}{I} \tag{1}$$

where "ρ" is sediment bulk density, "μ" is the Compton attenuation coefficient, "d" is the sediment thickness and "I_0" and "I" are the gamma intensity of the source and measured through the sample, respectively. To generate high quality density data, corrections must be implemented for experimental factors such as water content, beam spreading and attenuation through the PVC core liner. We took an empirical approach to calibrating the gamma density measurements by using half-cylinder aluminum calibration tubes of varying thicknesses that resembled the split peat cores (Fig. SI-1). Gamma counts were measured for 100 s along the calibration tubes that were encased in PVC core liners and filled with water. The average densities at different thicknesses were then calculated using the following equation:

$$\rho_{av} = \left(\frac{d_i}{D}\right) * \rho_{Al} + \frac{(D - d_i)}{D} * \rho_{water} \tag{2}$$

where "ρ_{av}" is the average density, "d_i" is the thickness of the aluminum calibration tube, "D" is total thickness and "ρ_{Al}" and "ρ_{water}" are the density of aluminum and water, respectively. The natural log of gamma intensities was then plotted against the average density of aluminum and water for various tube thicknesses ($\rho_{av} \times d$ vs. $ln (cps)$). The best-fit line through the measured values deviated from the theoretical line (Fig. SI-2) as a function of the variables mentioned above. The multi-sensor was calibrated for measuring wet bulk density using the following empirically-derived equation and the Gamma ray attenuation counts from the Neor peat core at increments of 1 cm and 10 s of integration time:

$$y = -0.07x + 8.8991 \tag{3}$$

where $y = ln(cps)$ and $x = \rho \times d$. Parameter d is the core thickness. Measurements of wet bulk density were performed on an adjacent core and transferred to the main core using the near-identical profiles of lithogenic elements. The dry bulk densities were calculated using the equation below and the water content of sub-samples extracted from the main core:

$$\rho_{dry} = \left(1 - \frac{Water \%}{100}\right) \times \rho_{wet} \tag{4}$$

where "ρ_{dry}" and "ρ_{wet}" are the dry and wet bulk densities respectively.

3.5. Total organic carbon (TOC) and stable isotope composition of organic carbon ($\delta^{13}C_{TOC}$)

Based on elemental variations identified using the XRF data, 400 sub-samples (average resolution of 30 Yr) were collected for TOC and δ^{13}C analyses. Between 0.002 and 0.015 g were sampled from 0.5 to 1.5 g of dried and homogenized peat material. Samples were transferred into pre-cleaned tin cups and treated with 10% HCl to remove inorganic carbon according to the procedure described in Hedges and Stern (1984). Total organic carbon was measured with a Thermo Scientific® Flash 2000 CHN analyzer at the Virginia Institute of Marine Science (VIMS). Quality control and data reproducibility procedures included analyzing duplicate samples and multiple acetanilide standards and use of an acetanilide standard

curve with a correlation coefficient (R^2) > 0.99. The $\delta^{13}C$ were determined at the RSMAS stable isotope laboratory (SIL) using a Costech elemental combustion system interfaced with a Thermo Scientific® Delta V Advantage continuous flow isotope ratio mass spectrometer. Reproducibility (<0.01‰) was assessed from repeated analysis of acetanilide and glycine standards.

3.6. Measurement of carbon accumulation rate

Changes in the Long Term Rate of Carbon Accumulation (LORCA), which is a function of carbon production and preservation, were calculated based on 71 samples (average resolution of ~118 Yr) following the method described in Tolonen and Turunen (1996) and using the following equation (Page et al., 2004):

$$LORCA\left(g\,C\,m^{-2}\,y^{-1}\right) = r \times 10000 \times \rho_{dry} \times c \tag{5}$$

where "r" is the average accumulation rate (mm y^{-1}), "ρ_{dry}" is dry bulk dry density (g cm^{-3}) and "c" is carbon content (g C g^{-1} dry weight).

3.7. Ti concentration and aeolian flux

In order to quantify the flux of dust to Neor peat mire over the last 13000 years, 60 samples (average resolution of ~220 Yr) were collected to be analyzed for Ti concentration. Approximately 0.2 g of peat material was transferred to capped, high-purity quartz crucibles and ashed in a muffle furnace at 750 °C for 1 h. Approximately 0.01 to 0.02 g of the ashed residue was transferred to a pre-cleaned 6-ml PFA Savillex vial and dissolved in 5 mL of concentrated HNO_3–HCl–HF mixture (2:2:1, volumetric ratios). The vials were placed in an ultrasonic bath for 2 h at 80 °C and then heated at 220 °C on a hotplate overnight. After complete digestion was achieved, about 0.1 g of the solution was diluted in 40 g of 0.45 mol L^{-1} HNO_3 and Ti concentration was measured against a mono-elemental standard solution (Spex CertiPrep) of known concentration (±5‰) by sample-standard-sample bracketing technique on the multi-collector inductively coupled plasma mass spectrometer (MC–ICPMS) at the Neptune Isotope Laboratory (NIL), RSMAS. Concentrations calculated based on ^{48}Ti, ^{49}Ti and ^{50}Ti isotopes were identical within uncertainties. The accuracy and precision of Ti measurements were evaluated by comparing three replicate analyses of USGS certified reference materials BCR-2 and BHVO-2 with 16 and 26 literature compilations (GEOREM, http://georem.mpch-mainz.gwdg.de/), respectively. Results for both reference materials agreed well with literature values within analytical uncertainties (Fig. SI-4). Contributions from the procedural blank were negligible (smaller than 0.1%). Nevertheless, corrections were applied to all measurements prior to calculating Ti concentrations.

Aeolian fluxes were calculated based on Ti concentrations in peat ash residues (Ti_{ash}) and assuming an average Ti concentration of 0.40% (4010 µg g^{-1}) in continental crust (Wedepohl, 1995) through the following equations (Bao et al., 2012):

$$Ti_{ash}\left(\mu g\,g^{-1}\right) = Ti\left(\mu g\,g^{-1}\right) \times \left(\frac{Ash(\%)}{100}\right)/(0.4) \tag{6}$$

$$Aeolian\,Flux\left(\mu g\,cm^{-2}y^{-1}\right) = Ti_{ash}\left(\mu g\,g^{-1}\right) \times \rho_{dry}\left(g\,cm^{-3}\right)$$
$$\times\,r\left(cm\,y^{-1}\right) \tag{7}$$

where "r": is the average accumulation rate (mm y^{-1}) and "ρ_{dry}" is the dry bulk density (g cm^{-3}) measured as described above.

3.8. Lipid extraction and n-alkane separation

Total lipids were extracted from approximately 1 g of 97 dried and homogenized peat samples (average resolution of ~140 Yr) with a solution of 2:1 dichloromethane:methanol (DCM/MeOH) using an Accelerated Solvent Extractor (Dionex ASE-200). The lipid extracts were partitioned into the organic phase following addition of methanol and NaCl-saturated water. Samples were concentrated to 1 ml using a Turbo-vap system under N_2 gas and half of the sample was used to separate n-alkanes from the remaining lipids through column chemistry. Samples were blown to "just dry" under N_2 and re-dissolved in hexane. Columns were packed with 5% water-deactivated silica gel (100–200 mesh) using hexane. Samples were eluted by three solvents, 10 mL of hexane, 10 mL of 25% toluene in hexane and 10 mL of MeOH. The first fraction was reduced to 0.5 mL under N_2 using the Turbo-vap. Concentrations of all n-alkanes present in the sample were identified using gas chromatography mass spectrometry (GC–MS) and individual n-alkanes were quantified relative to an internal standard (5α-cholestane). The abundance of hydrophilic floating and submerged plants (medium chain n-alkanes: C_{23}, C_{25}) relative to terrestrial plants (characterized by long chain n-alkane: C_{29}, C_{31}) was quantified according to "$P_{aqueous}$" (P_{aq}) ratio employing the equation below (Ficken et al., 2000):

$$P_{aq} = (C_{23} + C_{25})/(C_{23} + C_{25} + C_{29} + C_{31}) \tag{8}$$

3.9. Compound-specific hydrogen isotope analysis

Alkanoic acids were separated from the total lipid extract of 39 samples (average resolution of ~340 Yr) using column chromatography (5 cm × 40 mm Pasteur pipette, NH_2 sepra bulk packing, 60 Å). Separation was achieved by eluting with 2:1 DCM:isopropanol, followed by 4% formic acid in diethylether, yielding neutral and acid fractions, respectively. The acid fraction was esterified with 5% HCl and 95% methanol of known isotopic composition at 70 °C for 12 h to yield corresponding fatty acid methyl esters (FAMEs). FAMEs were obtained by liquid-liquid-extraction using hexane as a non-polar solvent, and traces of water picked up during sample processing were removed by passing the sample through a column of anhydrous Na_2SO_4. FAMEs were further purified using column chromatography (5 cm × 40 mm Pasteur pipette, 5% water-deactivated silica gel, 100–200 mesh), eluting with hexane, followed by FAMEs eluted with DCM.

Compound specific hydrogen isotopic values were obtained using gas chromatography isotope ratio mass spectrometry (GC–IRMS). We used a Thermo Scientific® Trace gas chromatograph equipped with a Rxi-5ms column (30 m × 0.25 mm, film thickness 1 µm) and a programmable temperature vaporizing (PTV) injector operated in solvent split mode with an evaporation temperature of 60 °C. The GC was connected via a GC Isolink with a pyrolysis furnace (at 1400 °C) via a Conflo IV interface to a DeltaVPlus isotope ratio mass spectrometer. The H_3^+-factor was determined daily to test linearity and accounted for 6.1 ppm mV^{-1} on average. Reference peaks of H_2 were co-injected between n-alkanoic acid peaks during the course of a GC–IRMS run; two of these peaks were used for standardization of the isotopic analysis, while the remainders were treated as unknowns to assess precision. Except for the case of co-elution, precision of these replicates was better than 0.6‰. The data were normalized to the VSMOW/SLAP hydrogen isotopic scale by comparing with an external standard containing 15 n-alkane compounds (C_{16} to C_{30}) with known δD values obtained from A. Schimmelmann, Indiana University,

Bloomington. The RMS error of replicate measurements of the standard across the course of analyses was 4.62 ± 0.83‰. We further monitored for instrument drift by measuring the δD values of a C_{34} n-alkane internal standard co-injected with the sample (240.6 ± 3.0‰; n = 105). The isotopic composition of H added during methylation of alkanoic acids was estimated by methylating and analyzing phthalic acid as a dimethyl ester (isotopic standard from A. Schimmelmann, University of Indiana) yielding $\delta D_{methanol}$ = −198.3‰ ± 3.9 (n = 7). Correction for H added by methylation was then made by way of mass balance.

3.10. Wavelet analysis

In order to track the degree of coherence between elemental pairs from the XRF measurements as a function of time, wavelet semblance analyses were performed following the continuous wavelet transform method (Cooper and Cowan, 2008) and using a modified MATLAB script. To identify the major periodicities within the time series, downcore variations of Ti abundances was decomposed into their major components using the complete ensemble empirical mode decomposition (CEEMD) approach (Torres et al., 2011). Subsequently, wavelet power spectrum analyses were performed on each individual component using the Morlet wave (Torrence and Compo, 1995) and a modified MATLAB script. We report notable periodicities according to the wavelet power spectra of each component, with global power spectra that exceed 1σ confidence level considered as significant periodicities. Prior to the analysis, each time series was detrended and linearly interpolated at a constant 3.5-year time step. To detrend the time series, the least-square best-fit line was subtracted from the original data by using the built-in MATLAB command. The 3.5-year time step closely approximates the average temporal sampling resolution of the XRF elemental data.

4. Results and discussion

4.1. The climate of the last deglaciation and the Holocene

4.1.1. Inorganic proxy record

The age model based on 19 calibrated radiocarbon dates is shown in Fig. 3, and the data are presented in Table 1. The average sedimentation rate (SR) calculated based on the age-depth model was 0.9 ± 0.6 (SD) mm Yr^{-1}, with the lowest rates dominating the early to mid-Holocene and the highest rates occurring after 1500 cal. Yr BP to the present (Fig. 3). Down-core abundances of Al, Zr, Ti, Si, Fe, K, and Rb measured by XRF-scanning at an average resolution of 3.5 Yr are shown in Fig. 4 along with a composite image of the 7.5 m peat core (see Table SI-1a for results). The light bands represent periods of high lithogenic (aeolian) input, while dark bands contain higher contents of decomposed organic matter. In general, the light bands dominated prior to the onset of the Holocene during the late Allerød and Younger Dryas periods. With the exception of several light bands that are evident between 8500—6500 cal. Yr BP, the period encompassing the early Holocene (*ca* 9000—6000 Yr BP) is dominated by dark organic matter. In contrast, the upper half of the core from around 6000 cal. Yr BP is marked with numerous and distinct bands of lithogenic material. It is evident from Fig. 4 that the relative abundances of refractory (Al, Zr, Ti, and Si), redox-sensitive (Fe) and mobile (K and Rb) elements covary throughout the entire record, with highest intensities corresponding to the light bands that contain high lithogenic content. Discrepancies are expected in the geochemical behavior of immobile elements compared with redox-sensitive and mobile elements if post-depositional mobilization and groundwater hydrochemistry affected the abundances of these elements during their
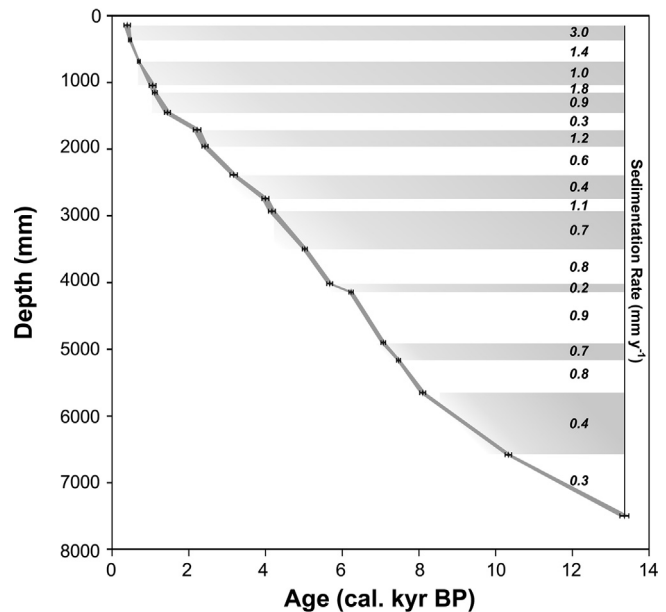

Fig. 3. The age model for the Neor peat core based on 19 calibrated AMS radiocarbon dates is shown. The narrow gray area between tie points refers to the 2σ uncertainty. Sedimentation rates (SR) between paired tie points are shown on the right axis. Sedimentation rates were calculated based on midpoint calibrated ages; see Table 1 for details.

depositional history. We observe significant correlations between the intensities of representative immobile (Ti), redox sensitive (Fe) and mobile (Rb) elements (Fe vs.Ti, R^2 = 0.81; Rb vs Ti, R^2 = 0.84, Fig. SI-3A, B). Additional confirmation comes from wavelet semblance analyses that show significant correlations among refractory conservative elements and both mobile and redox sensitive elements as a function of time, indicating that mineral dust particles have not been mobilized since deposition, and the ombrotrophic nature of the peat has been sustained throughout the record (Fig. SI-3C—H). Taken together along with the absence of any significant riverine input to this high-altitude peat mire, we attribute elevated intensities of lithogenic elements to enhanced aeolian input of mineral dust to the study area.

The record of lithogenic input as represented by Ti intensities (Fig. 5A) captures at least eleven abrupt episodes of enhanced aeolian deposition that lasted from several decades to millennia. Six of these events correspond to major Holocene rapid climate change (HRCC) periods associated with changes in the chemistry of the Greenland Ice Sheet ice core (GISP2) that were correlated to the record of globally distributed glacier fluctuations during the Holocene (Fig. 5A and J) (see Mayewski et al., 2004 and references therein). As noted by Mayewski et al. (2004), however, the HRCC events are not necessarily limited to these six episodes but rather these periods provide an overarching framework against which Holocene palaeoclimate records can be placed in regional and hemispheric context.

Strong evidence for an atmospheric teleconnection between the climate of the North Atlantic and the interior of West Asia comes from the agreement between the dust record from Neor and the expansion of the Siberian Anticyclone inferred from elevated K^+ ion concentrations in the GISP2 ice core (Mayewski et al., 1997) (Fig. 5I), as well as Holocene ice rafted debris (IRD) events from North Atlantic sediments (arrows 1—9 in Fig. 5A) (Bond et al., 1997), which are also associated with intervals of reduced solar irradiance (Bond et al., 2001). Shifts to more arid conditions found in records from the eastern Mediterranean Sea (Kaniewski et al., 2010; Migowski

Table 1
Radiocarbon dates and calibrated ages.

Sample no.	Depth ±5 mm[a]	Conventional age (RCYBP) ±reported error[b]	Midpoint calibrated age (year BP) ±2σ error	Midpoint calibrated age (Calendar year) ±2σ error
NES3-1-21	138	335 ± 30	393 ± 84	1557 ± 84 AD
NES3-1-2	361	385 ± 25	467 ± 39	1483 ± 39 AD
NES3-1-3	683	760 ± 35	699 ± 36	1251 ± 36 AD
NES3-2-4	1044	1140 ± 35	1055 ± 89	895 ± 89 AD
NES3-2-22	1150	1180 ± 25	1114 ± 61	836 ± 61 AD
NES3-2-5	1449	1540 ± 30	1443 ± 78	510 ± 78 AD
NES3-2-6	1710	2180 ± 30	2215 ± 99	266 ± 99 AD
NES3-3-7	1956	2400 ± 35	2422 ± 79	473 ± 79 BC
NES3-3-8	2384	2990 ± 30	3170 ± 95	1221 ± 95 BC
NES3-3-9	2740	3670 ± 30	3997 ± 90	2048 ± 90 BC
NES3-4-24	2930	3780 ± 35	4166 ± 90	2217 ± 90 BC
NES3-4-10	3497	4450 ± 30	5024 ± 64	3075 ± 64 BC
NES3-5-26	4017	4950 ± 40	5672 ± 75	3724 ± 75 BC
NES3-5-12	4143	5390 ± 35	6230 ± 56	4281 ± 56 BC
NES3-6-13	4900	6220 ± 35	7070 ± 60	5121 ± 60 BC
NES3-6-14	5166	6550 ± 40	7468 ± 50	5519 ± 50 BC
NES3-6-15	5653	7290 ± 35	8098 ± 77	6149 ± 77 BC
NES3-7-17	6583	9180 ± 70	10,331 ± 85	8423 ± 85 BC
NES3-8-20	7500	11,500 ± 50	13,356 ± 116	11,407 ± 116 BC

[a] Indicates the error on depth measurement.
[b] RCYP = Radiocarbon year before present. Uncertainty calculations are according to the National Ocean Sciences Accelerator Mass Spectrometry Facility (NOSAMS) radiocarbon data and calculation protocol at http://www.whoi.edu/nosams.

et al., 2006; Schilman et al., 2001) are also coincident with episodes of enhanced aeolian input from our record, and further indicate a climate coupling with the northern hemisphere (Fig. 5J).

Changes in the intensities of lithogenic elements measured by XRF provide a qualitative account of aeolian input. We quantified the flux of dust over the entire record by measuring downcore concentrations of Ti in discrete samples at an average resolution of ~220 Yr/sample (Table SI-1b). The relative changes in Ti intensities measured by XRF at high resolution and dust fluxes based on the Ti concentrations of discrete samples are in good agreement throughout the record (Fig. 5 A−B). Higher abundances of Ti coincide with increases in dust flux by one to more than two orders of magnitude (Fig. 5B, Table SI-1c). The maximum dust fluxes observed in the record were 510 and 545 μg cm^{-3} y^{-1} centered at 12230 and 5200 cal. Yr BP, respectively and the minimum value was 3 μg cm^{-3} y^{-1} centered at 3450 cal. Yr BP. From the beginning of the record at 13356 cal. Yr BP up to 10340 cal. Yr BP, dust fluxes ranged between 510 and 100 μg cm^{-3} y^{-1}. Dust fluxes are low during most of early Holocene with an episodic high input of 290 μg cm^{-3} y^{-1} around 8000 cal. Yr BP. The mid-late Holocene is highlighted by several dust events with fluxes ranging from 10 to 545 μg cm^{-3} y^{-1}, with the highest flux around 5200 cal. Yr BP.

Elemental variations in the Neor peat core (Figs. 4 and 5A−B) indicate that the most recent period of deglaciation is marked by a gradual increase in the intensities of lithogenic elements and aeolian fluxes from the Allerød period to the Younger Dryas, followed by a decline in aeolian input until around 10200 cal. Yr BP. We note that dust fluxes declined by nearly fivefold from the highest values during the Younger Dryas to the early Holocene (Fig. 5B). With the exception of two episodes of elevated dust from 8350−7900 and 7650−7400 cal. Yr BP, less dust was deposited prior to and during the early Holocene relative to the last deglacial period and mid-late Holocene. Episodes of enhanced dust deposition from 8500 to 6300 cal. Yr BP (Fig. 5A−B) coincide with times of reduced rainfall and strong solar minima as recorded in stalagmites from the Hoti cave, Oman (Neff et al., 2001). The prolonged period of dust deposition from 6300 to 5000 cal. Yr BP is in good agreement with the termination of the African Humid Period in subtropical Africa between 6000 and 5000 cal. Yr BP (deMenocal et al., 2000; Gasse and Van Campo, 1994). Episodes of low dust input during the

mid-Holocene around 5700 and 6000 cal. Yr BP also coincide with wet periods in eastern Mediterranean as recorded in stalagmites from Soreq Cave in Israel (Bar-Matthews and Ayalon, 2011).

Enhanced aeolian input is more frequent as summer solar insolation at 60 °N declines (Fig. 5A) after around 6000 cal. Yr BP to the present. These episodes are also coincident with drier conditions as recorded in palaeoclimate archives from Lake Tecer in Turkey (Kuzucuoglu et al., 2011) and Maharlou and Zeribar Lakes in Iran (Djamali et al., 2009; Griffiths et al., 2001; Wasylikowa and Witkowski, 2008; see Fig. 5J). Our results support the findings of a recent compilation of aeolian fluxes from 43 palaeodust records over the last 12000 Yr that suggest minimum mineral dust deposition during the early to mid-Holocene (Albani et al., 2015).

4.1.2. Organic proxy records and dust source variability

The picture that emerges from the lithogenic input to Neor peat mire is corroborated by variations in TOC content and δ^{13}C of bulk organic matter. At a resolution of 30 Yr/sample, the δ^{13}C$_{TOC}$ range from −28.7 to −25.3‰, with more negative values corresponding with lower TOC and higher abundances of Ti since 9800 cal. Yr BP (Fig. 5A and C−D). This suggests that drier conditions coincided with lower production and/or lower preservation of organic matter during dustier periods. Although variations in sedimentation rate can potentially influence TOC, a strong covariation is observed between TOC, δ^{13}C$_{TOC}$ and the relative abundances of Ti, which suggests that the TOC record is not significantly biased by changes in accumulation rates. We note that the relationship between δ^{13}C$_{TOC}$ and TOC is less evident between 11500 and 8000 cal. Yr BP, and apparently becomes decoupled from XRF intensities of Ti prior to 11500 cal. Yr BP. While we cannot offer a straightforward explanation for this decoupling, it is likely due to a change in plant assemblage/species and the hydrological regime during the transition from glacial to interglacial conditions. The dominant plant species in the Neor peat mire is *Drepanocladus* sp. moss (*D. aduncus − polygamous*), a highly polymorphic species typical of periodically flooded bogs that are subjected to environmental modifications (Harald Kürschner, Freir Universität Berlin, Institut für Biologie, Systematische Botanik und Pflanzengeographie, unpublished data).

Additional evidence for changes in the hydrological regime during the deglacial period and Holocene comes from the hydrogen
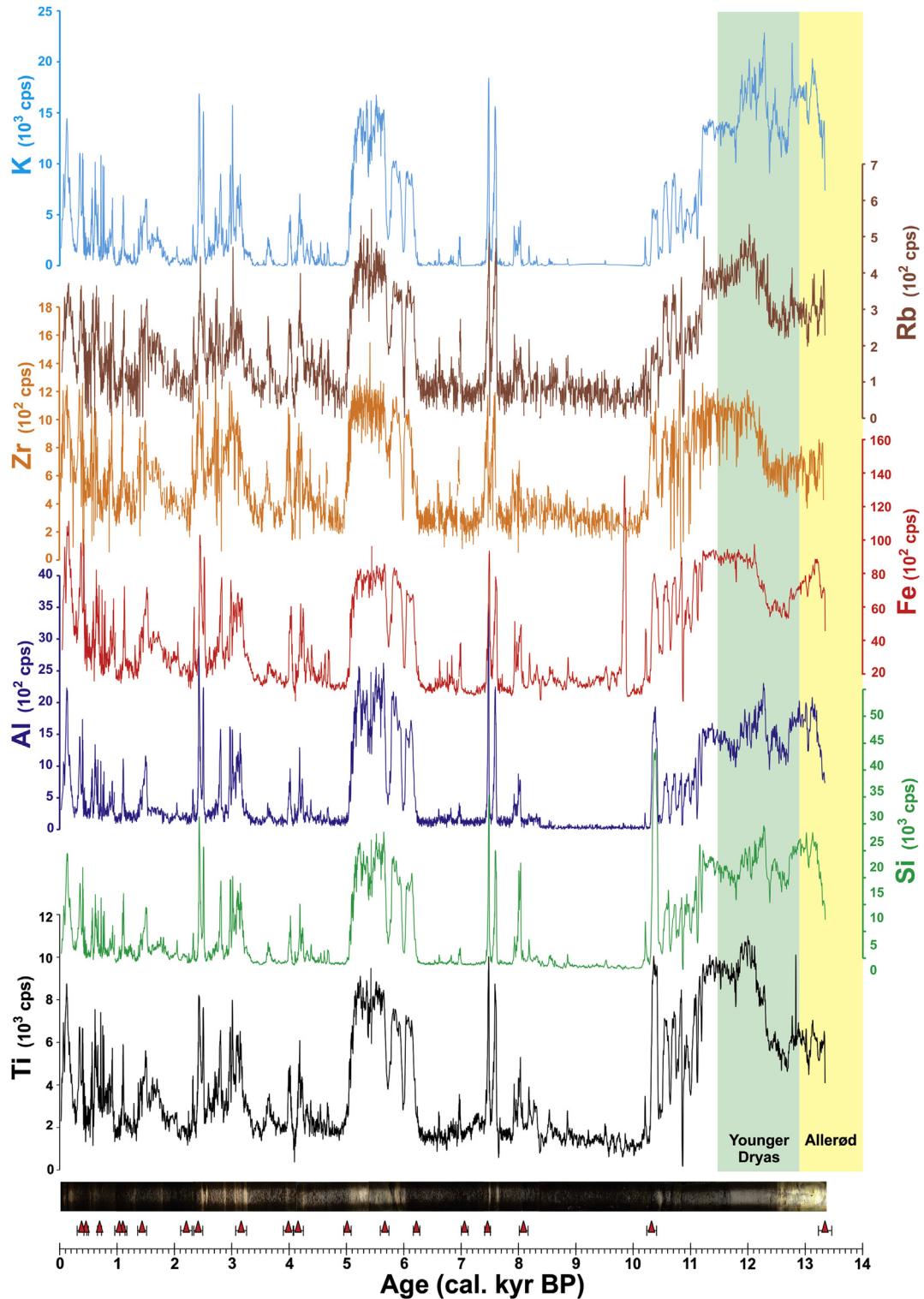
Fig. 4. Downcore XRF profiles of elemental abundances for refractory lithogenic (Al, Zr, Ti, and Si) and redox sensitive (Fe) and mobile (K and Rb) elements in counts per second (cps) associated with major dust intervals (light bands) over the last 13356 cal. Yr BP at Neor peat mire. The red triangles denote the stratigraphic position of calibrated radiocarbon dates measured on bulk samples. Light bands in the core image correspond with peaks of lithogenic elements. Dark bands are mainly comprised of decomposed organic matter with low intensities of lithogenic elements.

isotopic composition (δD) of C_{28} *n*-alkanoic acid (Fig. 5E). The average monthly δD of precipitation in the interior of West Asia is correlated with average monthly precipitation at two meteorological stations located 1365 km to the west and 390 km to the east of the Neor peat mire at the same latitude (Fig. 6). Changes in δD measured on 39 samples (340 Yr/sample resolution, Table SI-1d) range from −225 to −185‰ with the most positive values observed during the Younger Dryas (−195 to −186‰), a time period also

represented by the highest input of lithogenic elements in the entire record as seen in the XRF-Ti profile and aeolian fluxes (Fig. 5A—B). In contrast, the most negative δD values are observed during the early Holocene, followed by a gradual increase around 8000−7000 cal. Yr BP to a plateau for the rest of the record (Fig. 5E). This agrees with reconstructions of water availability based on chironomid assemblages in Neor peat mire during the Younger Dryas and the early Holocene (Aubert, 2013), as well as some of the records (particularly oxygen isotopes) from Lake Zeribar (Stevens et al., 2001) in west Iran that documented a wet early Holocene period followed by drier conditions (Fig. 5J). A similar shift from enriched δ18O values during Younger Dryas to more negative values during early Holocene is observed in most of the records from Mediterranean lakes (Roberts et al., 2008), indicating wet conditions prevailed in the region during early Holocene. These records are consistent with the influence of high solar insolation (Fig. 5A) during the early Holocene.

Transition from the most positive δD values during the Younger Dryas to the most negative δD values during the early Holocene, followed by a return to more positive values during the middle to late Holocene indicate that moisture availability, moisture source, or most likely a combination of both varied between these time periods, with the wettest interval during the early Holocene. This observation is further supported by the maximum in carbon accumulation rates of up to 13 g C m^{-3} y^{-1} (Fig. 5A, E and G). The lowest carbon accumulation rates are observed during the Younger Dryas and other periods of high dust input, while higher carbon accumulation rates are associated with periods of low dust input throughout the record. Although absolute values differ as would be expected between climatic regions, a similar trend of δD-enrichment across the Holocene is also observed in leaf wax δD composition measured in sediments of Lake Victoria (Berke et al., 2012), Lake Tanganika (Tierney et al., 2008) in East Africa (Fig. 5H), as well as in other records of hydrological changes in the African Tropics (Gasse, 2000). Moisture delivery to northwest Iran and eastern Africa during the early Holocene likely occurred through different synoptic systems; enhanced summer monsoon over east Africa and the position of the subtropical westerly jet and westerly disturbances over NW Iran. Expansion of moisture from the Caspian Sea is another possibility. Neor peat mire, however, is located on the leeward side of the Alborz Mountain Range, a natural barrier that retains moist air masses from the Caspian Sea (Fig. 1). Nevertheless, the similarities in δD records of leaf wax between Neor peat mire and East African Lakes, especially Lake Victoria, are indicative of a hemispheric forcing mechanism, most likely changes in solar insolation that influenced the climate of tropical and subtropical Africa and Eurasia (deMenocal et al., 2000; deMenocal and Tierney, 2012).

In addition to carbon accumulation rates and δD records, the Paq index, used as a proxy for the dominance of submerged vs emergent plants, provide a measure of water availability in peat mires (Seki et al., 2009; Zhou et al., 2005, 2002). Although the Paq index (Fig. 5F, Table SI-1e) are highly variable from sample to sample (not shown) and do not show a wide range, the highest mean value for Paq was observed during the early Holocene (Fig. 5F). In comparison, the average Paq during the middle and late Holocene were progressively lower, suggesting the declining dominance of submerged plants, most likely due to diminishing moisture availability as solar insolation declined. While carbon accumulation rates, the Paq index and compound-specific δD point to substantial changes in moisture availability and/or shifts in the hydrological regime during the last 13000 years over the study area, they do not allow us to differentiate between potential changes in the path/source of moisture brought from the Mediterranean Sea via subtropical westerlies and westerly disturbances (Alijani and Harman, 1985;

Alijani, 2002) the Caspian Sea, the Persian Gulf and Arabian and the Red Sea regions (Evans and Smith, 2006; Raziei et al., 2013, 2012), especially during the early Holocene.

The potential change in source is not limited to water. The clustering of lithogenic elements (Ca, Al, Si) into three distinct groups (Fig. 7) raises the possibility of shifts in the source(s) of aeolian material during the late Termination to early and mid-late Holocene. Indeed, preliminary results of geochemical fingerprinting with radiogenic Sr−Nd−Hf isotope systematics and rare earth element anomalies measured in mineral dust from Neor peat, paired with simulations of atmospheric circulation have shown shifts in dust source provenances during these periods that may be related to the meridional migration of the main axis of the subtropical Westerly jet over the study area as a result of changes in solar insolation over the northern Hemisphere (Sharifi et al., in preparation).

4.1.3. Wavelet analysis and periodicities in aeolian input

Wavelet power spectrum analysis conducted on major components of the Ti intensity time series for the entire record (13356 years, Fig. 8) reveal six centennial to millennial periodicities. Peaks centered on the power spectra of ~230, ~320 and ~470 years are notable but not significant (global power spectrum below 1σ). These periodicities are close to the de Vries cycle of solar excursions (~210 yr; Steinhilber et al., 2012) and ~520 yr (un-named cycle). Significant periodicities over the entire record are centered at~820, ~1550, and ~3110 years and are similar to a 1000 Yr (Eddy cycles; Abreu et al., 2010) cycle based on ^{14}C in tree-rings and solar activity records (Stuiver and Braziunas, 1991), and the 1500 and 3000 years cycles in solar irradiance (Bond et al., 2001, 1997). Given the length of the entire record, however, the 3000 year periodicity should be treated with caution.

Previous studies in the Arabian Sea, an area significantly impacted by the Indian Ocean summer monsoon, have shown a strong atmospheric teleconnection between the North Atlantic and northern Indian Ocean on millennial timescales during the last glacial period (Altabet et al., 2002; Pourmand et al., 2005, 2007, 2004; Schulz et al., 1998). Taken together, the correlations between our multi-proxy records and other archives from the eastern Mediterranean Sea, African lakes, Greenland (GISP2) (deMenocal et al., 2000; deMenocal and Tierney, 2012; Turner et al., 2008), and the results from wavelet analysis of aeolian input to Neor peat mire point to changes in solar irradiance and insolation on Holocene climate variability, and suggest an atmospheric teleconnection between the North Atlantic and the interior of West Asia during the last glacial termination and the present interglacial period.

4.2. Climate change and human societies in West Asia during the mid-late Holocene

Archaeological and historical records from West Asia have documented rise and fall of human societies across the eastern Mediterranean, Mesopotamia and northern Persian Gulf (e.g. Brooks, 2006; Cullen et al., 2000; deMenocal, 2001; Riehl, 2009). Nevertheless, little is known about the influence of rapid climate change on human societies due to the scarcity of high-resolution palaeoclimate reconstructions with robust age models, and the gaps in the historical and archaeological records, which are also prone to uncertainties. As a step towards a better understanding of the potential relationship between rapid climate change and human responses in this region, we compare our findings with a compilation of historical and archaeological records of drought, famine, socio-economic and cultural transitions over the Iranian Plateau (Iran), Mesopotamia (MSP), and eastern Mediterranean
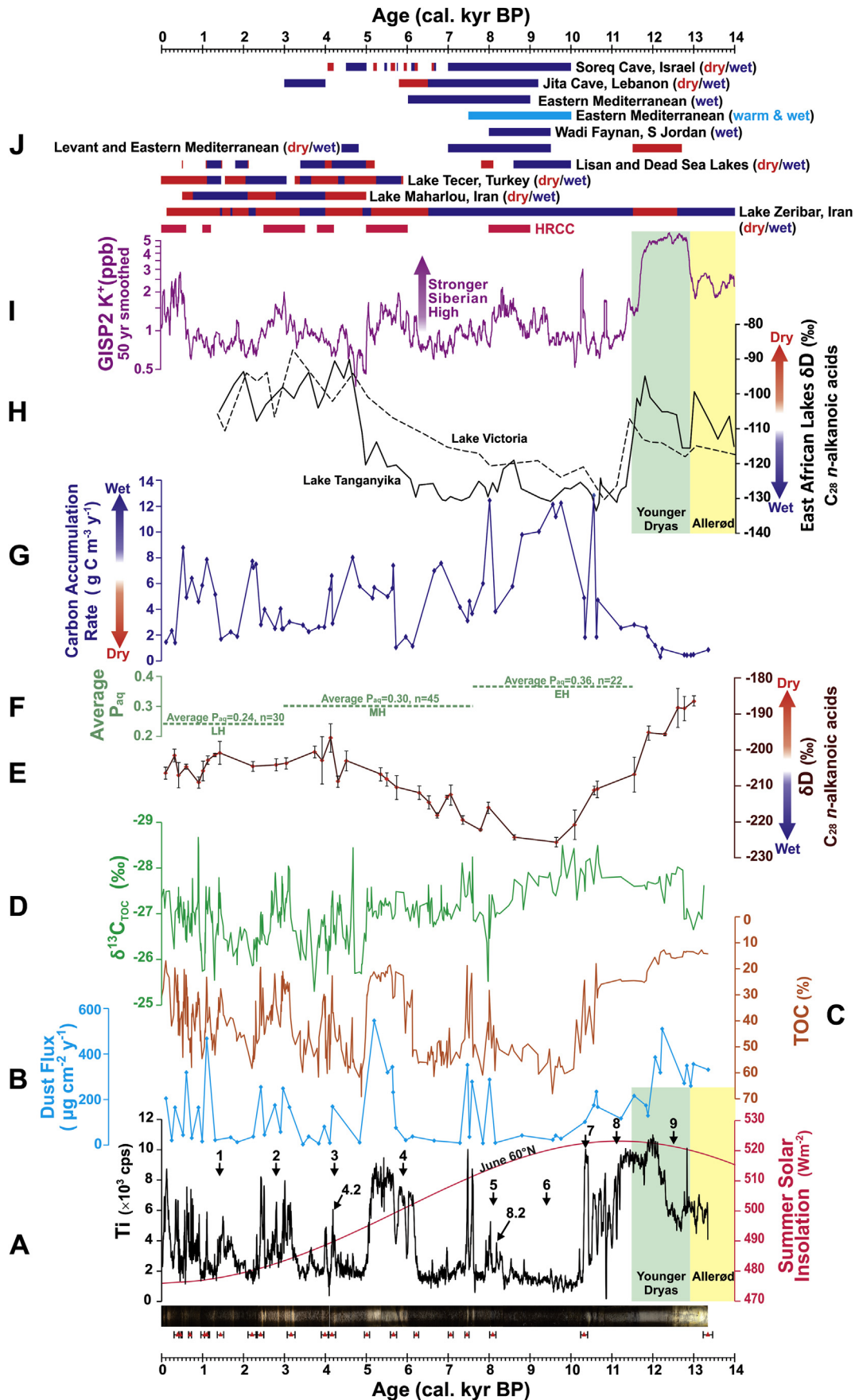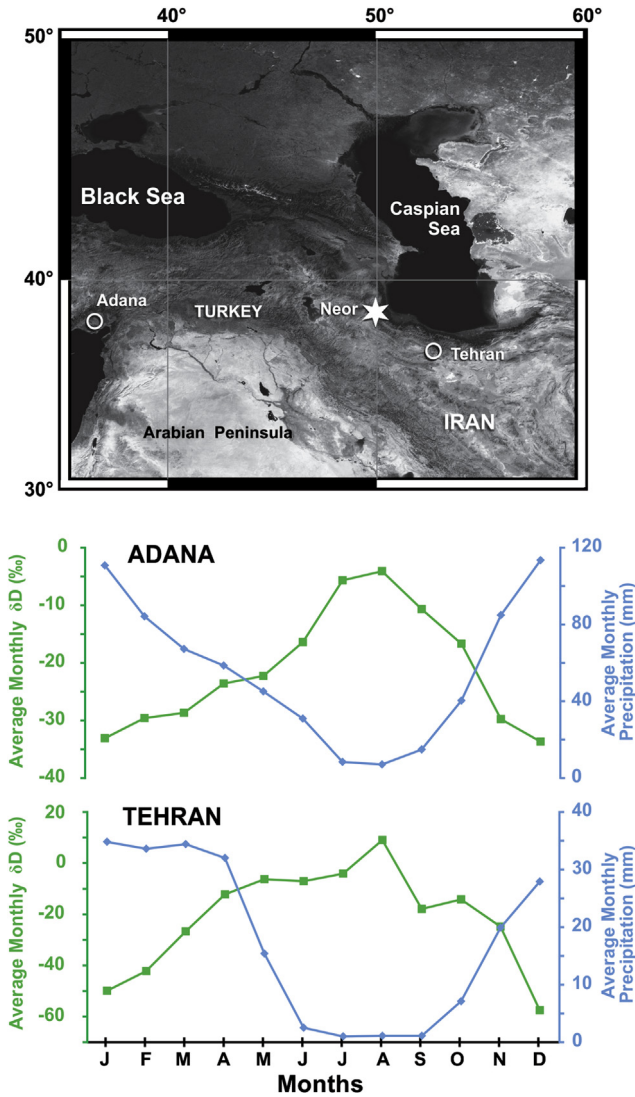
Fig. 6. Average monthly δD is strongly correlated with monthly precipitation at the two synoptic station in Turkey ($R^2 = 0.93$ at Adana, 36-year average) and Iran ($R^2_{Iran,Jan-Aug} = 0.66$ at Tehran, 44-year average). Source: Global Network of Isotopes in Precipitation (GNIP), http://www.univie.ac.at/cartography/project/wiser/.
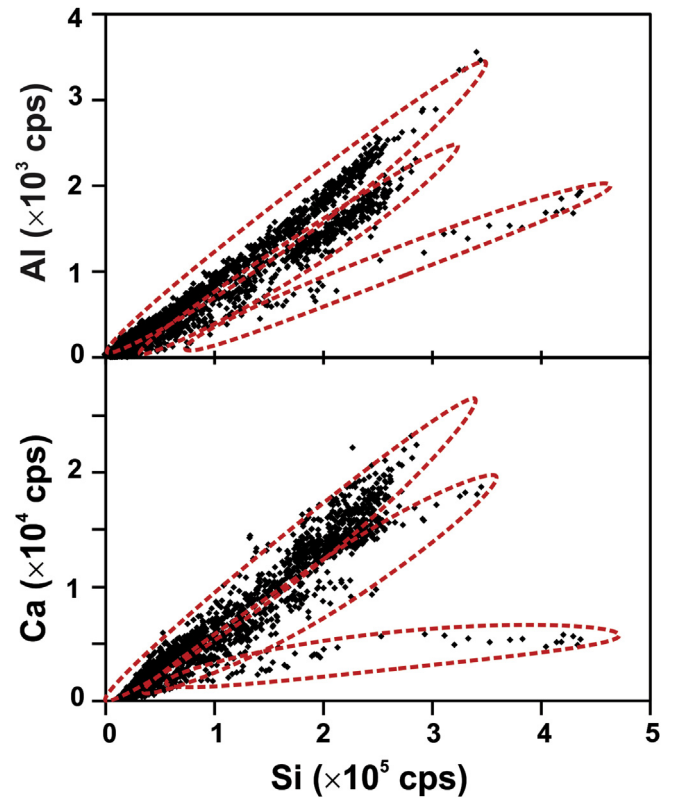

Fig. 7. XRF-abundances of Al ($\times 10^3$ cps) and Ca ($\times 10^4$ cps) with respect to Si ($\times 10^5$ cps) in Neor peat core. Areas identified with dotted line denote major clustering groups of potentially different source provenances.

(EM) regions along with palaeoclimate records of dry/wet periods for West Asia (see Table SI-2 and SI-3).

The rugged terrain of the Iranian Plateau was likely not as hospitable to societal development compared to epicenters of development across the Fertile Crescent where sociocultural developments evolved within river valleys (e.g. Egypt). In addition, interpretation of archaeological records across the Iranian Plateau is challenging because unequal attention has been paid to different locations and even different historical periods (Abdi, 2011). Although some artifacts of early settlements and the onset of agriculture in the region date back to ~12000 Yr BP (Riehl et al.,

2013) and despite the records of early villages in Iran as early as 9000 Yr BP (7000 BC), the nomadic-sedentary dichotomy did not appear till the early Bronze Age (ca. 3200 to 2200 BC) (Abdi, 2011). Transition from food procurement to food production societies in Mesopotamia took place around 5000 BP, when irrigated cultivation yielded surpluses that led to increased population and formation of the first city-units, the central entity in the rise of early Near Eastern civilizations (Childe, 1950; Redman, 1978). Middle Bronze Age (ca. 2200 to 1600 BC) in the Iranian Plateau is highlighted by florescence of urbanism (Abdi, 2011). As a result, we compare these records with the high-resolution aeolian input from Neor between 5000 cal. Yr BP to present (2010) with considerations for uncertainties in our age model (Fig. 9). Note that we do not incorporate the age uncertainties that are inherent in historical and archaeological records but are not reported or often difficult to establish.

With these caveats in mind, we note eight episodes of high aeolian input that mostly coincided with dry conditions in other regional palaeoclimate records (Fig. 9A and F). These episodes also coincided with accounts of drought, famine, socio-economic and cultural transitions over Iran, MSP, and EM regions. Most notably, we confirm evidence from a marine core that suggested the fall of the Akkadian Empire at 4200 Yr BP was coincident with an episode

Fig. 5. Multi-proxy sediment record in Neor peat from NW Iran. (A) core image (750-cm), 19 radiocarbon dates and Ti ($\times 10^3$ cps) intensity profile measured by XRF are shown along with summer solar insolation (Wm-2) at 60° N (red line), North Atlantic Holocene Ice Rafted Debris (IRD) 1–9 (Bond et al., 1997), and 4.2, 8.2 cooling events (Bond et al., 1997). (B) Dust flux based on Ti concentration ($\times 10$ µg cm^{-3} y^{-1}). (C) Total organic carbon (TOC)%. (D) Bulk δ^{13}C of TOC, TOC and δ^{13}C$_{TOC}$ are plotted in reverse scale. (E) Compound-specific δD (‰). (F) The average of Paq index during early (EH), middle (MH) and late Holocene (LH). (G) Carbon accumulation rate (g C cm^{-3} y^{-1}). (H) Compound-specific δD (‰) values for Lake Tanganyika (solid line) (Tierney et al., 2008) and Lake Victoria (Berke et al., 2012) (dashed line) in East Africa. (I) Variations in K$^+$ ion concentration from GISP2 ice core as a proxy for changes in the strength of the Siberian Anticyclone (Mayewski et al., 1997) and (J) Compilation of Mesopotamian and Mediterranean palaeoclimate records. Bars in magenta denote Holocene rapid climate change events (HRCC) (Mayewski et al., 2004); see text and Table SI-2 for details.
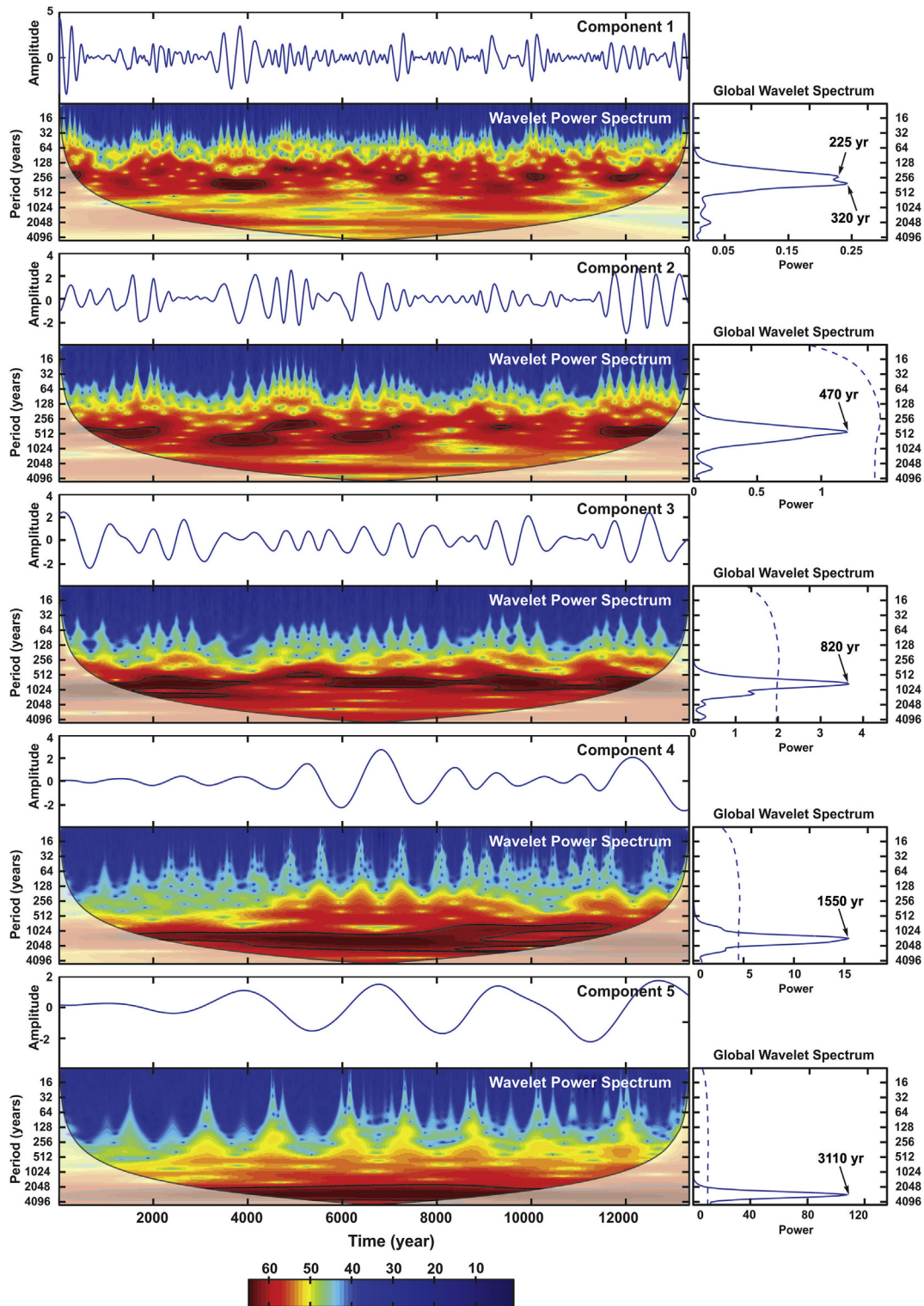
Fig. 8. Wavelet power spectrum of the major components of detrended time series of Ti intensities using the Morlet wavelet (Torrence and Compo, 1995) and complete ensemble empirical mode decomposition (CEEMD) approach (Torres et al., 2011). White areas denote the cone of influence and black boundaries mark 1σ confidence level. The color bar refers to the wavelet power values from dark blue (low values), to dark red (high values).The global power spectrum with the most significant peaks of spectral power is shown on the right panel, dashed lines are refer to 1σ confidence level.

of exceptionally high aeolian input to the Arabian Sea (Cullen et al., 2000). Further, transitions in major Mesopotamian and Iranian civilizations, including the collapse of the Ur III empire at 3955 Yr BP (Leick, 2010), the fall of the Elam empire at 2800 Yr BP, and the Medes empire at 2500 Yr BP, as well as the demise of the Achaemenids around 2280 Yr BP, the Partians around 1730 Yr BP, the Sasanians at 1300 Yr BP, and the Safavids at 950 Yr BP (Daryaee, 2011), overlapped with major dust events from this study (Fig. 9F

and G). Periods of prolonged drought from 4550 to 2800 cal. Yr BP and several short droughts from 2100 to 100 cal. Yr BP in Iran, MSP and EM are also coincided with episodes of enhanced dust deposition from our record (Fig. 9B, C, and F). Drought events during the period of 1800–1500 cal. Yr BP in Iran were followed by famine (Fig. 9B, and C). Other events in Iran after 1300 cal. Yr BP, which have been associated with war, political tensions and resource crisis (Table SI-3), also coincided with high levels of atmospheric dust

deposition (Fig. 9C, and F) at Neor. Consecutive drought events from 1770 to 1930 AD recorded in central Anatolia also coincided with the latest major dust event from our record (200 BP to present).

We emphasize, however, that historical and archaeological accounts of societal change are lacking during some periods of elevated atmospheric dust (Fig. 9). This suggests that either climate change did not significantly impact the human societies in the region during those periods, or the communities were better
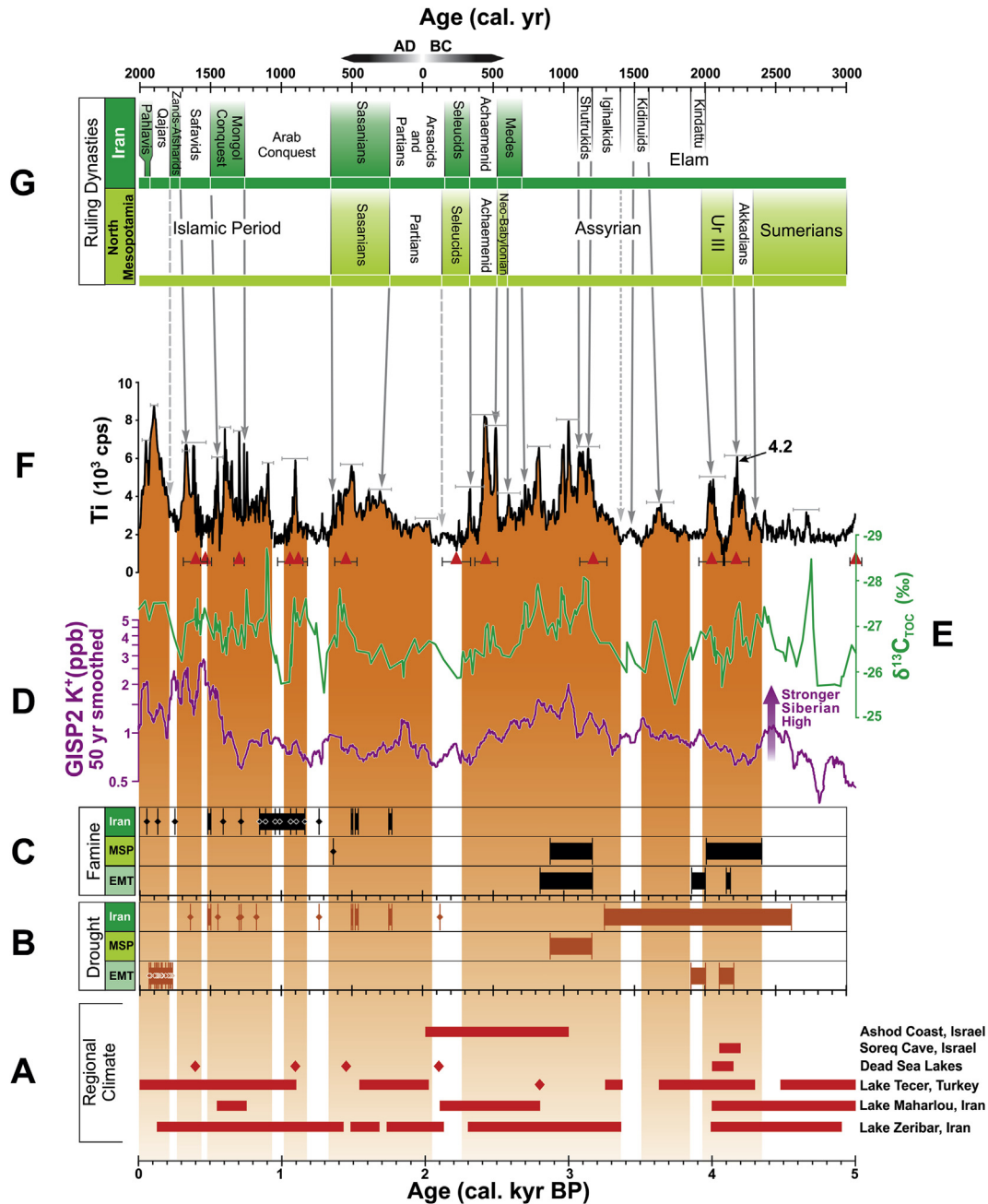

Fig. 9. Periods of enhanced aeolian deposition from Neor peat core compared with cultural transitions and historical and archaeological accounts of climate change in West Asia over the last 5000 Yr. (A) Episodes of dry conditions as recorded in regional palaeoclimate data are from Ashod Coast, Israel; Soreq Cave, Israel; Lisan and Dead Sea Lakes; Lake Tecer, Turkey; Lake Maharlou, Iran, and Lake Zeribar, Iran. (B) Drought records from Iran, MSP and EM since 3000 BC; bars and diamonds refer to prolonged and single drought events, respectively. (C) Historical records of prolonged (bars) and single (diamonds) famine events from Iran, MSP and EM since 3000 BC. For data on panels A through C see Tables SI2 and 3. (D) Variations in K+ ion concentration from GISP2 ice core as a proxy for changes in the strength of the Siberian Anticyclone. (E) Bulk $\delta^{13}C_{TOC}$ plotted in reverse scale. (F) Ti intensity (cps) over the last 5000 Yr. Data for panels D through F are presented in Table SI1. The error bars on major peaks approximate the uncertainties associated with the age model in this study interpolated from two adjacent age tie points. Red triangles are calibrated radiocarbon dates and Orange areas denote major episodes of dust deposition since 5000 cal. Yr BP. The 4.2 kyr event coinciding with the Collapse of the Akkadian Empire is also shown. (G) Ruling dynasties in Iran (top) and Mesopotamia (bottom) since 3000 BC (~5000 BP). Gray arrows denote power transitions.

equipped to adjust to abrupt changes. Alternatively, it is possible that accounts of these events were not recorded or are missing from historical and archaeological archives due to the power transition between ruling governments. Nevertheless, given that agriculture, livestock and timber production dominated the economies of early civilizations in this region (Zohary and Hopf, 2000), climate change can be expected to have played a significant role in the development of human societies and in power transitions. While we made every effort to compile notable historical and archaeological archives, some records may be missing from this compilation and should be further considered in future comparisons.

As a final remark, we note that while abrupt climate change may have influenced human societies across the region, it is reasonable to expect that increasing human activities in the form of deforestation and agropastoral land use may have, in turn, contributed to elevated eolian content of the atmosphere as these activities are known to expose soil material to erosion and transport by wind (Eastwood et al., 1999; Vermoere et al., 2002). A recent study on the fossil pollen and insect remains from a peripheral peat core in NE part of the lake (Fig. 1) suggest that pastoralism was likely practiced in the high elevation surroundings of Neor in Talysh Mountains ~6000 Yr BP (Ponel et al., 2013). The authors also conclude that on a regional scale, agropastoral activities intensified after about 2000 Yr BP. In another study, Djamali (2009b) identified several phases of intensified human activities based on pollen records of the last 3500 years from a crater peat record located about 175 km SW of our study area.

Major dust events of the last 5000 years in Neor broadly covary with the intensity of the Siberian anticyclone, and the peaks of high eolian input are followed by a shift in $\delta^{13}C_{TOC}$ and TOC (Fig. 9D and E, see also Fig. 5C, D and I). These proxies are independent of human activities and suggest drier conditions prevailed during the episodes of enhanced dust input. Indeed, the δD data during the last 3000 years are relatively constant, indicating little or no change in moisture availability during these high-dust input events. This observation suggests that although human activity may have contributed to additional dust during the last 3000 years, as implied by numerous high-frequency events over this period (Fig. 5), this most likely happened in the broader context of abrupt climate change that was already underway. It is worth mentioning that based on satellite observations of dust optical depth from MODIS measurements (Ginoux et al., 2012), anthropogenic sources in modern times account for up to 25% of global dust emission, with significant spatial variability. Dust emissions due to human activities were likely lower during late Holocene than they are today. The contribution from natural *vs* anthropogenically-introduced aeolian sources and the extent to which human activities affected climate change in the region cannot be fully addressed with the current dataset and additional high-resolution proxy reconstructions that can be linked to specific human activities based on historical and archeological records in the region are needed to assess this hypothesis.

5. Conclusions

We present a high-resolution reconstruction of aeolian input and changes in palaeoenvironmental conditions from a 13000 year peat record from NW Iran. Variation in elemental abundances, TOC, $\delta^{13}C_{TOC}$, compound-specific leaf wax hydrogen isotopes (δD), carbon accumulation rates and aeolian fluxes revealed that dry and dusty conditions prevailed during the late glacial termination. This period was followed by a wetter and less dusty interval during the early Holocene over the interior of West Asia. Subsequently, the middle-late Holocene became drier and marked by higher

frequency intervals of aeolian input to the study area. The multi-proxy dataset presented in this study supports the interpretation that low $\delta^{18}O$ values from lakes in western Iran correspond to wetter conditions during the early Holocene.

Comparison with regional records and wavelet analysis of aeolian input to Neor peat mire suggest changes in solar insolation (and possibly irradiance) most likely played a key role in controlling water availability and aeolian input to the studied region. Our data also suggest an atmospheric teleconnection existed between North Atlantic climate and West Asia during the last glacial termination and the Holocene. Nearly all episodes of enhanced deposition of lithogenic material in our record corresponded with episodes of drought and famine in the region as well as with transitions in major Mesopotamian and Iranian civilizations. This includes the fall of the Akkadian empire around 4200 Yr BP as was previously suggested from marine sediments of the Arabian Sea. Our findings indicate that ancient human societies from West Asia were likely highly susceptible to abrupt climate variability during the current interglacial period. The extent to which human activities across the region influenced soil erosion and created new sources of eolian material for proximal and distant transport during the last 3000 years remains to be constrained as more high-resolution reconstructions become available from West Asia.

Appendix A. Supplementary data

Supplementary data related to this article can be found at http://dx.doi.org/10.1016/j.quascirev.2015.07.006.

References

Abdi, K., 2011. The Iranian plateau from paleolithic times to the rise of the Achaemenid empire. In: Daryaee, T. (Ed.), The Oxford Handbook of Iranian History. Oxford University Press Inc., p. 400

Abreu, J.A., Beer, J., Ferriz-Mas, A., 2010. Past and future solar activity from cosmogenic radionuclides. SOHO-23 Work Underst. Peculiar Sol. Minim. 428, 287–295.

Albani, S., Mahowald, N.M., Winckler, G., Anderson, R.F., Bradtmiller, L.I., Delmonte, B., François, R., Goman, M., Heavens, N.G., Hesse, P.P., Hovan, S.A., Kohfeld, K.E., Lu, H., Maggi, V., Mason, J.A., Mayewski, P.A., McGee, D., Miao, X., Otto-Bliesner, B.L., Perry, A.T., Pourmand, A., Roberts, H.M., Rosenbloom, N., Stevens, T., Sun, J., 2015. Twelve thousand years of dust: the Holocene global dust cycle constrained by natural archives. Clim. Past. Discuss. 11, 869–903. http://dx.doi.org/10.5194/cp-11-869-2015.

Alijani, B., 2002. Variations of 500 hPa flow patterns over Iran and surrounding areas and their relationship with the climate of Iran. Theor. Appl. Climatol. 72, 41–54.

Alijani, B., Harman, J., 1985. Synoptic climatology of precipitation in Iran. Ann. Assoc. Am. Geogr. 75, 404–416.

Altabet, M.A., Higginson, M.J., Murray, D.W., 2002. The effect of millennial-scale changes in Arabian Sea denitrification on atmospheric CO_2. Nature 415, 159–162.

Aubert, C., 2013. Changements environnementaux et climatiques en Iran à la transition Tardiglaciaire/Holocène: apport des assemblages fossiles de Chironomideae (Insectes, Diptères) de la séquence lacustre de Neor au nord-ouest de l'Iran (altitude 2480 m). Institut Méditerranéen de Biodiversité et d'Ecologie.

Bao, K., Xing, W., Yu, X., Zhao, H., McLaughlin, N., Lu, X., Wang, G., 2012. Recent atmospheric dust deposition in an ombrotrophic peat bog in Great Hinggan

Mountain. Northeast China. Sci. Total Environ. 431, 33−45. http://dx.doi.org/10.1016/j.scitotenv.2012.05.014.

Bar-Matthews, M., Ayalon, A., 2011. Mid-Holocene climate variations revealed by high-resolution speleothem records from Soreq Cave, Israel and their correlation with cultural changes. Holocene 21, 163−171. http://dx.doi.org/10.1177/0959683610384165.

Berke, M.A., Johnson, T.C., Werne, J.P., Grice, K., Schouten, S., Sinninghe Damsté, J.S., 2012. Molecular records of climate variability and vegetation response since the Late Pleistocene in the Lake Victoria basin, East Africa. Quat. Sci. Rev. 55, 59−74. http://dx.doi.org/10.1016/j.quascirev.2012.08.014.

Boelter, D.H., 1966. Important physical properties of peat materials. In: Proceeding of the Third International Peat Congress. Quebec, pp. 150−154.

Bond, G., Kromer, B., Beer, J., Muscheler, R., Evans, M.N., Showers, W., Hoffmann, S., Lotti-Bond, R., Hajdas, I., Bonani, G., 2001. Persistent solar influence on North Atlantic climate during the Holocene. Science 294, 2130−2136. http://dx.doi.org/10.1126/science.1065680.

Bond, G., Showers, W., Cheseby, M., Lotti, R., Almasi, P., Priore, P., Cullen, H., Hajdas, I., Bonani, G., 1997. A pervasive millennial-scale cycle in North Atlantic Holocene and glacial climates. Sci. (80) 278, 1257−1266.

Brooks, N., 2006. Cultural responses to aridity in the Middle Holocene and increased social complexity. Quat. Int. 151, 29−49. http://dx.doi.org/10.1016/j.quaint.2006.01.013.

Chambers, F.M., Beilman, D.W., Yu, Z., 2011. Methods for determining peat humification and for quantifying peat bulk density, organic matter and carbon content for palaeostudies of climate and peatland carbon dynamics. Mires Peats 7, 1−10.

Childe, V.G., 1950. The urban revolution. Town Plan. Rev. 21, 3−17.

Connor, S.E., Kvavadze, E.V., 2008. Modelling late Quaternary changes in plant distribution, vegetation and climate using pollen data from Georgia. Cauc. J. Biogeogr. 36, 529−545. http://dx.doi.org/10.1111/j.1365-2699.2008.02019.x.

Cooper, G.R.J., Cowan, D.R., 2008. Comparing time series using wavelet-based semblance analysis. Comput. Geosci. 34, 95−102. http://dx.doi.org/10.1016/j.cageo.2007.03.009.

Cullen, H.M., deMenocal, P.B., Hemming, S., Hemming, G., Brown, F.H., Guilderson, T., Sirocko, F., 2000. Climate change and the collapse of the Akkadian empire: evidence from the deep sea. Geology 28, 379 doi:10.1130/0091-7613(2000)28<379:CCATCO>2.0.CO;2.

Daryaee, T., 2011. The Oxford Handbook of Iranian History, first ed. Oxford University Press Inc., New York.

deMenocal, P., Ortiz, J., Guilderson, T., Adkins, J., Sarnthein, M., Baker, L., Yarusinsky, M., 2000. Abrupt onset and termination of the African Humid Period : rapid climate responses to gradual insolation forcing. Quat. Sci. Rev. 19, 347−361.

deMenocal, P.B., 2001. Cultural responses to climate change during the late holocene. Sci. (80) 292, 667−673. http://dx.doi.org/10.1126/science.1059287.

deMenocal, P.B., Tierney, J.E., 2012. Green Sahara: african humid periods paced by earth's orbital changes. Nat. Educ. Knowl. 3, 12.

Djamali, M., Akhani, H., Andrieu-Ponel, V., Braconnot, P., Brewer, S., de Beaulieu, J.-L., Fleitmann, D., Fleury, J., Gasse, F., Guibal, F., Jackson, S.T., Lezine, A.-M., Medail, F., Ponel, P., Roberts, N., Stevens, L., 2010. Indian summer monsoon variations could have affected the early-Holocene woodland expansion in the Near East. Holocene 20, 813−820. http://dx.doi.org/10.1177/0959683610362813.

Djamali, M., Beaulieu, J.-L., Miller, N.F., Andrieu-Ponel, V., Ponel, P., Lak, R., Sadeddin, N., Akhani, H., Fazeli, H., 2009a. Vegetation history of the SE section of the Zagros Mountains during the last five millennia: a pollen record from the Maharlou Lake, Fars Province, Iran. Veg. Hist. Archaeobot. 18, 123−136. http://dx.doi.org/10.1007/s00334-008-0178-2.

Djamali, M., de Beaulieu, J.-L., Andrieu-Ponel, V., Berberian, M., Miller, N.F., Gandouin, E., Lahijani, H., Shah-Hosseini, M., Ponel, P., Salimian, M., Guiter, F., 2009b. A late Holocene pollen record from Lake Almalou in NW Iran: evidence for changing land-use in relation to some historical events during the last 3700 years. J. Archaeol. Sci. 36, 1364−1375. http://dx.doi.org/10.1016/j.jas.2009.01.022.

Eastwood, W.J., Roberts, N., Lamb, H.F., Tibby, J.C., 1999. Holocene environmental change in southwest Turkey: a palaeoecological record of lake and catchment-related changes. Quat. Sci. Rev. 18, 671−695. http://dx.doi.org/10.1016/S0277-3791(98)00104-8.

El-Moslimany, P., 1982. The late Quaternary vegetational history of the Zagros and Taurus Mountains in the regions of Lake Mirabad, Lake Zeribar, and Lake Van — a reappraisal. In: Bintliff, J.L., Zeist, W. Van (Eds.), Palaeoclimates, Palaeoenvironments and Human Communities in the Eastern Mediterranean Region in Later Prehistory, pp. 275−540. Part II. British Archaeological Reports, Oxford.

Evans, H.B., 1965. GRAPE — a device for continuous determination of material density and porosity. In: Trans. 6th Annu. SPWLA Logging Symp. II, B, pp. 1−25.

Evans, J.P., Smith, R.B., 2006. Water vapor transport and the production of precipitation in the Eastern fertile crescent. J. Hydrometeorol. 7, 1295−1307. http://dx.doi.org/10.1175/JHM550.1.

Ficken, K.J., Li, B., Swain, D.L., Eglinton, G., 2000. An n-alkane proxy for the sedimentary input of submerged/-oating freshwater aquatic macrophytes. Org. Geochem. 31.

Gasse, F., 2000. Hydrological changes in the African tropics since the Last Glacial Maximum. Quat. Sci. Rev. 19, 189−211. http://dx.doi.org/10.1016/S0277-3791(99)00061-X.

Gasse, F., Van Campo, E., 1994. Abrupt post-glacial climate events in West Asia and North Africa monsoon domains. Earth Planet. Sci. Lett. 126, 435−456.

Ginoux, P., Prospero, J.M., Gill, T.E., Hsu, N.C., Zhao, M., 2012. Global-scale attribution of anthropogenic and natural dust sources and their emission rates based on Modis deep blue aerosol products. Rev. Geophys. 50, 1−36. http://dx.doi.org/10.1029/2012RG000388.

Griffiths, H.I., Schwalb, A., Stevens, L.R., 2001. Environmental change in southwestern Iran: the Holocene ostracod fauna of Lake Mirabad. Holocene 11, 757−764. http://dx.doi.org/10.1191/09596830195771.

Grootes, P.M., Stuiver, M., White, J.W.C., Johnsen, S., Jouzel, J., 1993. Comparison of oxygen isotope records from the GISP2 and GRIP Greenland ice cores. Nature 366, 552−554. http://dx.doi.org/10.1038/366552a0.

Hedges, J., Stern, J., 1984. Carbon and nitrogen determinations of carbonate-containing solids. Limnol. Oceanogr. 29, 657−663.

Janssens, J.A., 1983. A quantitative method for stratigraphic analysis of bryophytes in Holocene peat. J. Ecol. 71, 189−196.

Kaniewski, D., Paulissen, E., Van Campo, E., Weiss, H., Otto, T., Bretschneider, J., Van Lerberghe, K., 2010. Late second-early first millennium BC abrupt climate changes in coastal Syria and their possible significance for the history of the Eastern Mediterranean. Quat. Res. 74, 207−215. http://dx.doi.org/10.1016/j.yqres.2010.07.010.

Kuzucuoglu, C., Dorfler, W., Kunesch, S., Goupille, F., 2011. Mid- to late-Holocene climate change in central Turkey: the Tecer Lake record. Holocene 21, 173−188. http://dx.doi.org/10.1177/0959683610384163.

Leick, G., 2010. Historical Dictionary of Mesopotamia, second ed. The Scarecrow Press, Inc., Lanham. Toronto. Plymouth. UK.

Madadi, A., Moghaddam, M.H.R., Rajaei, A.H., 2005. Study of the geomorphological evolution of the Neor Lake in Ardabil region, NW Iran. Quat. J. Geogr. Res. 1−12 (in Persian).

Mayewski, P.A., Meeker, L.D., Twickler, M.S., Lyons, W.B., Prentice, M., 1997. Major features and forcing of high-latitude northern hemisphere atmospheric circulation using a 110,000-year-long glaciochemical series. J. Geophys. Res. 102, 26,345−26,366.

Mayewski, P.A., Rohling, E.E., Stager, J.C., Maasch, K.A., Meeker, L.D., Meyerson, E.A., Gasse, F., Kreveld, S. Van, Holmgren, K., Lee-thorp, J., Rosqvist, G., Rack, F., Staubwasser, M., Schneider, R.R., Steig, E.J., 2004. Holocene climate variability. Quat. Res. 62, 243−255. http://dx.doi.org/10.1016/j.yqres.2004.07.001.

Mellaart, J., 1975. The Neolithic of the Near East. Charles Scribner's Sons, New York.

Migowski, C., Stein, M., Prasad, S., Negendank, J.F.W., Agnon, A., 2006. Holocene climate variability and cultural evolution in the Near East from the Dead Sea sedimentary record. Quat. Res. 66, 421−431. http://dx.doi.org/10.1016/j.yqres.2006.06.010.

Neff, U., Burns, S.J., Mangini, a, Mudelsee, M., Fleitmann, D., Matter, a, 2001. Strong coherence between solar variability and the monsoon in Oman between 9 and 6 kyr ago. Nature 411, 290−293. http://dx.doi.org/10.1038/35077048.

Nicoll, K., Küçükuysal, C., 2013. Emerging multi-proxy records of Late Quaternary Palaeoclimate dynamics in Turkey and the surrounding region. Turk. J. Earth Sci. 22, 126−142. http://dx.doi.org/10.3906/yer-1109-7.

Page, S.E., Wūst, R.A.J., Weiss, D., Rieley, J.O., Shotyk, W., Limin, S.H., 2004. A record of Late Pleistocene and Holocene carbon accumulation and climate change from an equatorial peat bog (Kalimantan, Indonesia): implications for past, present and future carbon dynamics. J. Quat. Sci. 19, 625−635. http://dx.doi.org/10.1002/jqs.884.

Ponel, P., Andrieu-ponel, V., Djamali, M., Lahijani, H., Leydet, M., Mashkour, M., 2013. Fossil beetles as possible evidence for transhumance during the middle and late Holocene in the high mountains of Talysch (Talesh) in NW Iran . J. Environ. Archeol. 18, 201−210.

Pourmand, A., Marcantonio, F., Bianchi, T.S., Canuel, E.A., Waterson, E.J., 2005. Radionuclide and biomarker proxies of past ocean circulation and productivity in the Arabian Sea. Geophys. Res. Lett. 32, 1−4. http://dx.doi.org/10.1029/2005GL022612.

Pourmand, A., Marcantonio, F., Bianchi, T.S., Canuel, E.A., Waterson, E.J., 2007. A 28-ka history of sea surface temperature, primary productivity and planktonic community variability in the western Arabian Sea. Paleoceanography 22. http://dx.doi.org/10.1029/2007PA001502. PA4208 1-14.

Pourmand, A., Marcantonio, F., Schulz, H., 2004. Variations in productivity and eolian fluxes in the northeastern Arabian Sea during the past 110 ka. Earth Planet. Sci. Lett. 221, 39−54. http://dx.doi.org/10.1016/S0012-821X(04)00109-8.

Razavi, T., Daryabari, J., Bordi, I., Pereira, L.S., 2013. Spatial patterns and temporal trends of precipitation in Iran. Theor. Appl. Climatol. 115, 531−540. http://dx.doi.org/10.1007/s00704-013-0919-8.

Razavi, T., Mofidi, A., Santos, J.A., Bordi, I., 2012. Spatial patterns and regimes of daily precipitation in Iran in relation to large-scale atmospheric circulation. Int. J. Climatol. 32, 1226−1237. http://dx.doi.org/10.1002/joc.2347.

Redman, C.L., 1978. The Rise of Civilization. W.H. Freeman and Company, San Francisco.

Reimer, P., Bard, E., Bayliss, A., 2013. IntCal13 and Marine13 radiocarbon age calibration curves 0−50,000 years cal BP. Radiocarbon 55, 1869−1887.

Riehl, S., 2009. Archaeobotanical evidence for the interrelationship of agricultural decision-making and climate change in the ancient Near East. Quat. Int. 197, 93−114. http://dx.doi.org/10.1016/j.quaint.2007.08.005.

Riehl, S., Zeidi, M., Conard, N.J., 2013. Emergence of agriculture in the foothills of the Zagros Mountains of Iran. Science 341, 65−67. http://dx.doi.org/10.1126/science.1236743.

Roberts, N., 2002. Did prehistoric landscape management retard the post-glacial spread of woodland in Southwest Asia? Antiquity 76, 1002—1010.

Roberts, N., Brayshaw, D., Kuzucuoglu, C., Perez, R., Sadori, L., 2011. The mid-Holocene climatic transition in the Mediterranean: causes and consequences. Holocene 21, 3—13. http://dx.doi.org/10.1177/0959683610388058.

Roberts, N., Jones, M.D., Benkaddour, A., Eastwood, W.J., Filippi, M.L., Frogley, M.R., Lamb, H.F., Leng, M.J., Reed, J.M., Stein, M., Stevens, L., Valero-Garcés, B., Zanchetta, G., 2008. Stable isotope records of Late Quaternary climate and hydrology from Mediterranean lakes: the ISOMED synthesis. Quat. Sci. Rev. 27, 2426—2441. http://dx.doi.org/10.1016/j.quascirev.2008.09.005.

Schilman, B., Bar-Matthews, M., Almogi-labin, A., Luz, B., 2001. Global climate instability reflected by Eastern Mediterranean marine records during the late Holocene. Palaeogeogr. Palaeoclimatol. Palaeoecol. 176, 157—176.

Schulz, H., von Rad, U., Erlenkeuser, H., 1998. Correlation between Arabian Sea and Greenland climate oscillations of the past 110,000 years: nature. Nature 393, 54—62.

Seki, O., Meyers, P.A., Kawamura, K., Zheng, Y., Zhou, W., 2009. Hydrogen isotopic ratios of plant wax n-alkanes in a peat bog deposited in northeast China during the last 16kyr. Org. Geochem 40, 671—677. http://dx.doi.org/10.1016/j.orggeochem.2009.03.007.

Sharifi, A., Pourmand, A., Murphy, L., Clement, A.C., Ahmadi Birgani, H., Naderi-Beni, A., Lahijani, H.A.K., 2015. Changes in dust sources and atmospheric circulation over Southwest Asia during the Holocene: insights from radiogenic Sr—Nd—Hf isotopes. REE Anomal. Clim. Simul. (in preparation).

Staubwasser, M., Weiss, H., 2006. Holocene climate and cultural evolution in late prehistoric — early historic West Asia. Quat. Res. 66, 372—387. http://dx.doi.org/10.1016/j.yqres.2006.09.001.

Steinhilber, F., Abreu, J.A., Beer, J., Brunner, I., Christl, M., Fischer, H., Heikkilä, U., Kubik, P.W., Mann, M., McCracken, K.G., Miller, H., Miyahara, H., Oerter, H., Wilhelms, F., 2012. 9,400 years of cosmic radiation and solar activity from ice cores and tree rings. Proc. Natl. Acad. Sci. USA 109, 5967—5971. http://dx.doi.org/10.1073/pnas.1118965109.

Stevens, L.R., Ito, E., Schwalb, A., Wright, H.E., 2006. Timing of atmospheric precipitation in the Zagros Mountains inferred from a multi-proxy record from Lake Mirabad. Iran. Quat. Res. 66, 494—500. http://dx.doi.org/10.1016/j.yqres.2006.06.008.

Stevens, L.R., Wright Jr., H.E., Ito, E., 2001. Proposed changes in seasonality of climate during the Lateglacial and Holocene at Lake Zeribar, Iran. Holocene 11, 747—755. http://dx.doi.org/10.1191/09596830195762.

Stuiver, M., Braziunas, T.F., 1991. Climatic, solar, oceanic, and geomagnetic influences on late-glacial and holocene atmospheric ^{14}C/^{12}C change. Quat. Res. 35, 1—24.

Stuiver, M., Reimer, P.J., Bard, E., Beck, J.W., Burr, G.S., Hughen, K.A., Kromer, B., McCormac, G., van der Plicht, J., Spurk, M., 1998. INTCAL98 radiocarbon age calibration, 24,000-0 cal BP. Radiocarbon 40, 1041—1083.

Tierney, J.E., Russell, J.M., Huang, Y., Damsté, J.S.S., Hopmans, E.C., Cohen, A.S., 2008. Northern hemisphere controls on tropical southeast African climate during the past 60,000 years. Science 322, 252—255. http://dx.doi.org/10.1126/science.1160485.

Tolonen, K., Turunen, J., 1996. Accumulation rates of carbon in mires in Finland and implications for climate change. Holocene 6, 171—178.

Torrence, C., Compo, G.P., 1995. A practical guide to wavelet analysis. Bull. Am. Meteorol. Soc. 79, 61—78.

Torres, E., Colominas, M.A., Schlotthauer, G., Flandrin, P., 2011. A complete ensemble empirical mode decomposition with adaptive noise. In: IEEE Int. Conf. on Acoust., Speech and Signal Proc. ICASSP-11, Prague (CZ). IEEE, Prague, pp. 4144—4147. CFP11ICA-ART.

Turner, R., Roberts, N., Jones, M.D., 2008. Climatic pacing of Mediterranean fire histories from lake sedimentary microcharcoal. Glob. Planet. Change 63, 317—324. http://dx.doi.org/10.1016/j.gloplacha.2008.07.002.

Vermoere, M., Bottema, S., Vanhecke, L., Waelkens, M., Paulissen, E., Smets, E., 2002. Palynological evidence for late-Holocene human occupation recorded in two wetlands in SW Turkey. Holocene 12, 569—584. http://dx.doi.org/10.1191/0959683602hl568rp.

Wasylikowa, E.K., Witkowski, A. (Eds.), 2008. Diatom Monographs. The Palaeoecology of Lake Zeribar and Surrounding Areas, Western Iran, during the Last 48,000 Years, vol. 8. A.R.G.Gantner Verlag K.G.

Wasylikowa, K., 2005. Palaeoecology of Lake Zeribar, Iran, in the Pleniglacial, Lateglacial and Holocene, reconstructed from plant macrofossils. Holocene 15, 720—735. http://dx.doi.org/10.1191/0959683605hl846rp.

Wasylikowa, K., Witkowski, A., Walanus, A., Hutorowicz, A., Alexandrowicz, S.W., Langer, J.J., 2006. Palaeolimnology of Lake Zeribar, Iran, and its climatic implications. Quat. Res. 66, 477—493. http://x.doi.org/10.1016/j.yqres.2006.06.006.

Wedepohl, K.H., 1995. The composition of the continental crust. Geochim. Cosmochim. Acta 59, 1217—1232.

Zhou, W., Lu, X., Wu, Z., Deng, L., Jull, A.J.T., Donahue, D., Beck, W., 2002. Peat record reflecting Holocene climatic change in the Zoigê Plateau and AMS radiocarbon dating. Chin. Sci. Bull. 74, 66—70.

Zhou, W., Xie, S., Meyers, P.A., Zheng, Y., 2005. Reconstruction of late glacial and Holocene climate evolution in southern China from geolipids and pollen in the Dingnan peat sequence. Org. Geochem. 36, 1272—1284. http://dx.doi.org/10.1016/j.orggeochem.2005.04.005.

Zohary, D., Hopf, M., 2000. Domestication of Plants in the Old World In: The Origin and Spread of Cultivated Plants in West Asia, Europe and the Nile Valley, third ed., vol. 3. Oxford University Press Inc., New York.